



A Kinetic Study on Selective Leaching of Phosphorus from Dephosphorization Slag

Chuan-ming Du¹ · Xu Gao^{2,3} · Shigeru Ueda³ · Shin-ya Kitamura³

Received: 16 August 2020 / Accepted: 19 October 2020 / Published online: 11 November 2020
© The Minerals, Metals & Materials Society 2020

Abstract

Phosphorus recovery from dephosphorization slag generated during steelmaking has enormous potential to secure a stable supply of phosphate. Because P and Fe in slag are concentrated in different mineral phases, P can be recovered by separation of the P-bearing phase, and the residue can be reutilized in steel plant at the same time. In the present study, we adopted selective leaching of P and investigated the effects of leaching parameters on the dissolution behavior of slag. It was determined that with the decrease in particle size and increase in stirring speed, the P dissolution ratio increased significantly. When particle size was less than 53 μm and stirring speed exceeded 200 rpm, most of the P-bearing $\text{C}_2\text{S}-\text{C}_3\text{P}$ solid solution was dissolved and separated. Increasing temperature and decreasing the mass ratio of slag to liquid had a slight influence on promoting P dissolution, while the Si dissolution was significantly suppressed in the case of high temperature and mass ratio due to the formation of silica gel. The P dissolution ratio reached 84.9%, and the Fe dissolution was negligible. Through selective leaching, the residue primarily consisting of magnesioferrite could be used as a flux in steelmaking process. The shrinking core model was successfully used to describe the dissolution kinetics of P. As temperature increased, apparent rate constant increased slightly. The calculated activation energy was 9.23 kJ/mol, demonstrating that the P dissolution was controlled by diffusion in the residue layer.

The contributing editor for this article was Hiromichi Takebe.

✉ Xu Gao
gao@tohoku.ac.jp

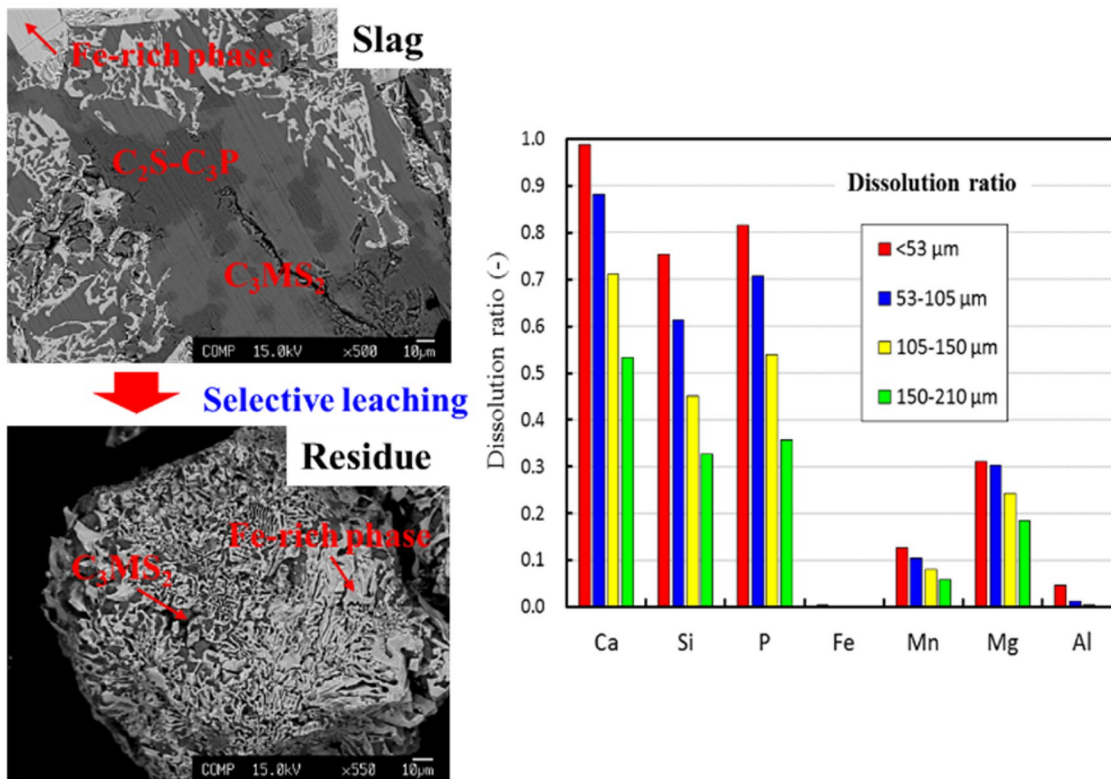
¹ School of Metallurgy, Northeastern University,
Shenyang 110819, China

² School of Metallurgy and Environment, Central South
University, Changsha 410083, P.R. China

³ Institute of Multidisciplinary Research for Advanced
Materials, Tohoku University, 2-1-1 Katahira, Aoba-ku,
Sendai 980-8577, Japan

Graphical Abstract

Most of the P-bearing solid solution in dephosphorization slag was dissolved and the dissolution of Fe-bearing phase was negligible, achieving selective leaching of P. The P dissolution from slag was controlled by diffusion in the residue layer.



Keywords Dephosphorization slag · Phosphorus recovery · C₂S–C₃P solid solution · Selective leaching · Kinetics

Introduction

Phosphorus (P) is a vital element for all living organisms, and a significant ingredient of commercial fertilizers. With the increase in the world's population, the agricultural sector requires large amounts of phosphate fertilizer to boost food production [1]. However, the reserve of high-grade phosphate ores, which is the primarily raw material to produce phosphate fertilizer, will be depleted in the future, and the price of phosphate ores is continuously increasing [2]. To secure a stable supply of P and achieve sustainable development of society, new phosphate sources urgently need to be exploited. Recently, considerable attentions have focused on P recovery from waste materials and industrial by-products, such as wastewater, sewage sludge, and slag [3–5].

In iron and steel industry, iron ores contain a small amount of phosphate, and the P content is increasing owing to the utilization of iron ores with a deteriorating quality [6]. Because P is a detrimental element in steel,

it is oxidized and removed from hot metal in steelmaking process by dephosphorization [7]. Dephosphorization slag principally consists of a CaO–SiO₂–Fe₂O₃ slag system, and the P₂O₅ content is approximately 3.0 mass% [8]. Although the P₂O₅ content in dephosphorization slag is far lower than that in phosphate ores, the total amount of P contained in slag is considerable because the annual production of steelmaking slag is huge, over 1.0 billion tones globally [9]. From another perspective, steel plant expects to remove P from slag because the existence of P₂O₅ hinders the reutilization of steelmaking slag as a flux or feedstock in metallurgical process [10]. If P₂O₅ can be effectively removed, it will not only reduce slag generation and save resources, but also make a great contribution to environmental protection. Therefore, separation and recovery of P from dephosphorization slag is considerably significant to both steel and phosphate industries.

In dephosphorization process with the multi-phase slag, the dephosphorization product of 3CaO·P₂O₅ reacts with the saturated 2CaO·SiO₂ to form a 2CaO·SiO₂–3CaO·P₂O₅ (C₂S–C₃P) solid solution [11]. Because most of the P₂O₅

was distributed in the C_2S-C_3P solid solution, P recovery from dephosphorization slag essentially depends on extraction of the C_2S-C_3P solid solution. Some methods aimed to extract solid solution from dephosphorization slag have been widely reported by using the difference in physicochemical properties between solid solution and other phases. Kubo et al. [12] investigated the recovery of the nonmagnetic solid solution from the Fe-bearing $CaO-SiO_2-Fe_2O_3$ phase in a strong magnetic field. Li et al. [13] proposed a method of super gravity to separate solid solution by using the difference in density. Koizumi et al. [14] studied the separation of the P-bearing $2CaO-SiO_2$ phase and Fe-bearing liquid phase by capillary action in the sintered CaO.

To efficiently extract a P-rich substance suitable for fertilizer production, Kitamura lab [15, 16] proposed selective leaching of the P-bearing solid solution from dephosphorization slag since it was readily soluble in a weak acid solution in comparison to other mineral phases. In previous studies [17–19], to achieve an improved selective leaching of P, slow cooling and oxidization of the molten slag was adopted to increase the dissolution ratio of C_2S-C_3P solid solution and suppress the dissolution of Fe-containing phases. It was determined that most of the P in slag was dissolved while the Fe dissolution ratio was very low. In view of the reutilization of residue and reducing production costs, we chose hydrochloric acid (HCl) which is readily available in industry as a leaching agent [20]. Following leaching, the phosphate dissolved in leachate was precipitated by adjusting pH, and then recovered as a substitute for phosphate rock which is widely used in fertilizer production [19]. The proposed process for comprehensive utilization of dephosphorization slag is shown in Fig. 1. By using selective leaching, no waste is discharged during steel-making and a new phosphate source is developed. Previous results adequately demonstrated that selective leaching, which was perceived as an efficient and low-cost method, exhibited

a technical advantage in P recovery from dephosphorization slag.

Although the effects of slag composition and treatment conditions on selective leaching of P have been studied, we have not yet investigated the leaching kinetics of P from dephosphorization slag. Therefore, in this work, we systematically studied the influences of dominating leaching parameters, such as particle size, temperature, stirring speed, and mass ratio of slag to liquid, on the dissolution behavior of slag at a constant pH in the HCl solution. The main objective of this study is to obtain the optimum leaching conditions for selective leaching of P, reveal the rate-limiting step, and provide theoretical basis for its future industrial application.

Materials and Method

Dephosphorization Slag Preparation

The synthesized dephosphorization slag whose composition is similar to industrial slag is used as raw material. Because the slag containing Fe_2O_3 exhibited a higher dissolution ratio of P [18], Fe_2O_3 was used as the iron oxide. As described in previous study [20], the mixed chemical reagents were put in a high-purity MgO crucible and heated to 1823 K to form a homogenous liquid slag in a resistance furnace. After holding at this temperature for 60 min, the molten slag was cooled to 1623 K at a speed of 3 K/min to precipitate solid solution. Then, the slag was cooled to 1273 K at a speed of 5 K/min and taken out of furnace. After cooling, the slag sample was crushed and sieved to collect various size fractions for the following acid leaching. The crystalline phases in dephosphorization slag were identified by X-ray diffraction (XRD). The morphology of slag and composition of mineral phases were determined by electron probe microanalysis (EPMA). The inductively coupled plasma-atomic emission spectrometry (ICP-AES) analysis after performing aqua-regia digestion was used for determining the concentration of target elements in slag. Using these results, we calculated the actual composition of synthesized slag, as listed in Table 1. This dephosphorization slag contains 3.29 mass% P_2O_5 and has a relatively low basicity.

Acid Leaching Experiments

As described in previous studies [17, 20], leaching experiment was carried out in a Teflon container with 400 mL of distilled water, which was immersed in a constant temperature water bath. The slag sample was ground and screened to

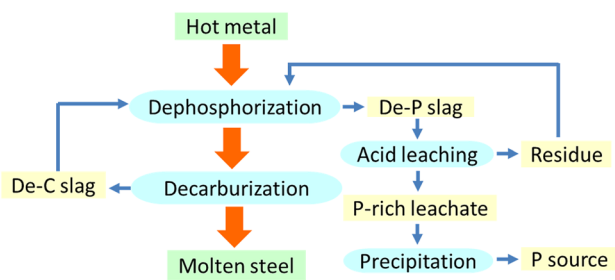


Fig. 1 Flowsheet of a waste-free steelmaking process

Table 1 Actual composition of the synthesized dephosphorization slag (mass%)

| Component | CaO | SiO ₂ | Fe ₂ O ₃ | P ₂ O ₅ | MgO | MnO | Al ₂ O ₃ |
|-----------|-------|------------------|--------------------------------|-------------------------------|-------|------|--------------------------------|
| Content | 31.19 | 19.86 | 27.79 | 3.29 | 10.24 | 4.58 | 3.05 |

different size portions (<53 μm , 53–105 μm , 105–150 μm , and 150–210 μm). Agitation was provided by mechanical stirring, with a stirring speed ranging from 20 to 300 rpm. The mass ratio of slag to solution varied from 1:100 to 1:10. During leaching, due to the increase of pH attributed to the Ca dissolution from slag, HCl solution was continuously added to the solution to decrease pH to a constant value by using a pH electrode and PC-controlled pump system. The optimum pH with a value of 3 determined previously was used in this study [20]. The leaching temperature ranged from 278 to 333 K. At selected time intervals, a certain amount (5 mL) of slurry was withdrawn and filtered by membrane filter (<0.45 μm). The concentrations of main elements in the filtered solution were analyzed using ICP-AES. After 120 min reaction, the slurry was filtered to collect residue. Following drying, the mass of residue was weighted, and its morphology and mineral composition were characterized by EPMA and XRD. The chemical composition of residue was determined using the same method for slag analysis.

Results

Mineral Composition of Dephosphorization Slag

The main components in dephosphorization slag were CaO, SiO₂, and Fe₂O₃, resulting in the formation of silicate

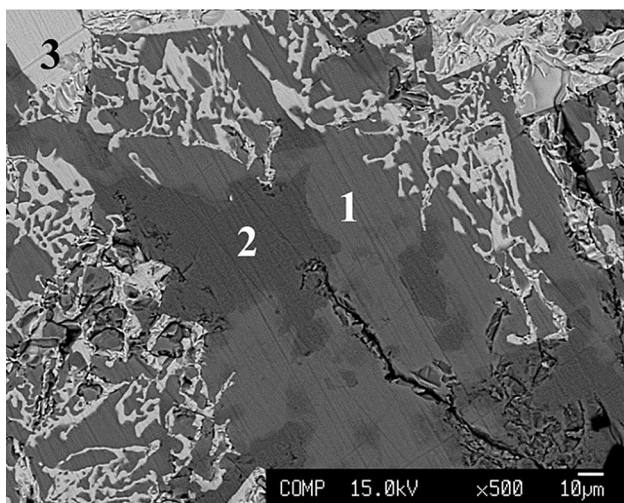


Fig. 2 EPMA image of the synthesized dephosphorization slag

Table 2 Average composition of each phase in dephosphorization slag (mass%)

| Phase | CaO | SiO ₂ | Fe ₂ O ₃ | P ₂ O ₅ | MgO | MnO | Al ₂ O ₃ |
|-------|------|------------------|--------------------------------|-------------------------------|------|-----|--------------------------------|
| 1 | 58.8 | 27.5 | 1.0 | 9.1 | 2.4 | 1.1 | 0.1 |
| 2 | 50.9 | 33.7 | 0.7 | 2.2 | 11.6 | 0.8 | 0.1 |
| 3 | 1.4 | 0.2 | 64.3 | 0.0 | 17.0 | 9.8 | 7.4 |

minerals and ferrite minerals. The typical morphology of mineral phases and their average chemical composition are presented in Fig. 2 and Table 2, respectively. The mineral phases were primarily categorized by three kinds of color (light gray, gray, dark gray). The light gray phase mainly containing Fe₂O₃ and MgO was regarded as magnesioferrite; the gray phase principally consisted of CaO, SiO₂, and MgO, with a rough molar ratio of 3.0:1.9:1.0, which was considered as merwinite [Ca₃Mg(SiO₄)₂]. The dark gray phase which primarily contained CaO and SiO₂ and had a relatively high P₂O₅ content was referred to as C₂S–C₃P solid solution. MnO and Al₂O₃ was mainly distributed in magnesioferrite which had extreme low contents of CaO and SiO₂. It was remarkable that P₂O₅ was concentrated in the C₂S–C₃P solid solution, and its content was approximately three times higher than that of average content in slag, while Fe₂O₃ was enriched in magnesioferrite. This difference is the fundamental factor that allows the separation of phosphorus and iron in slag.

Dissolution Characteristic of Dephosphorization Slag

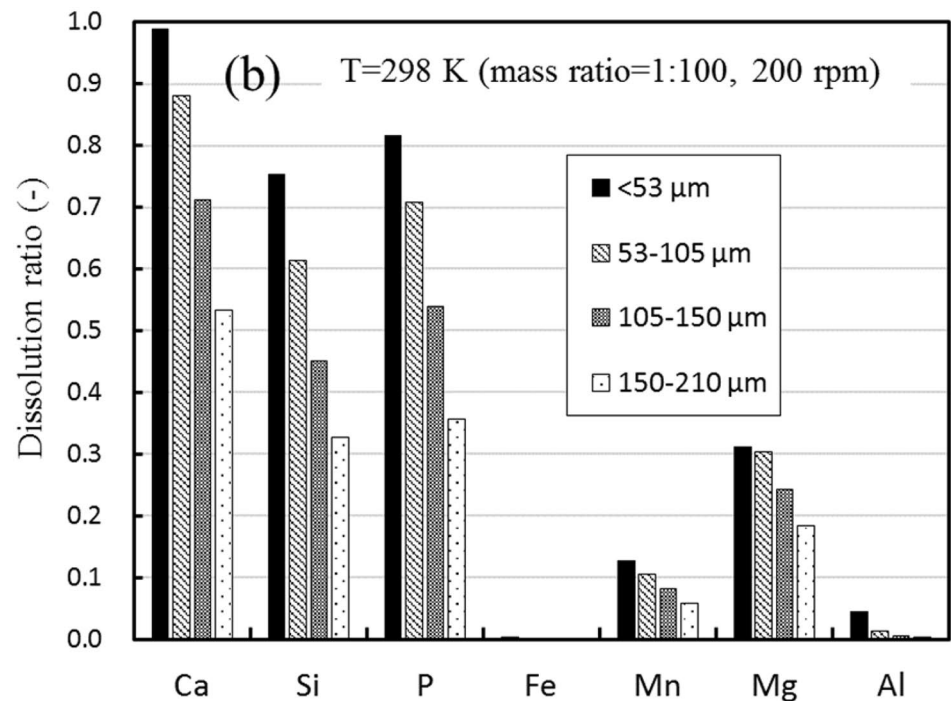
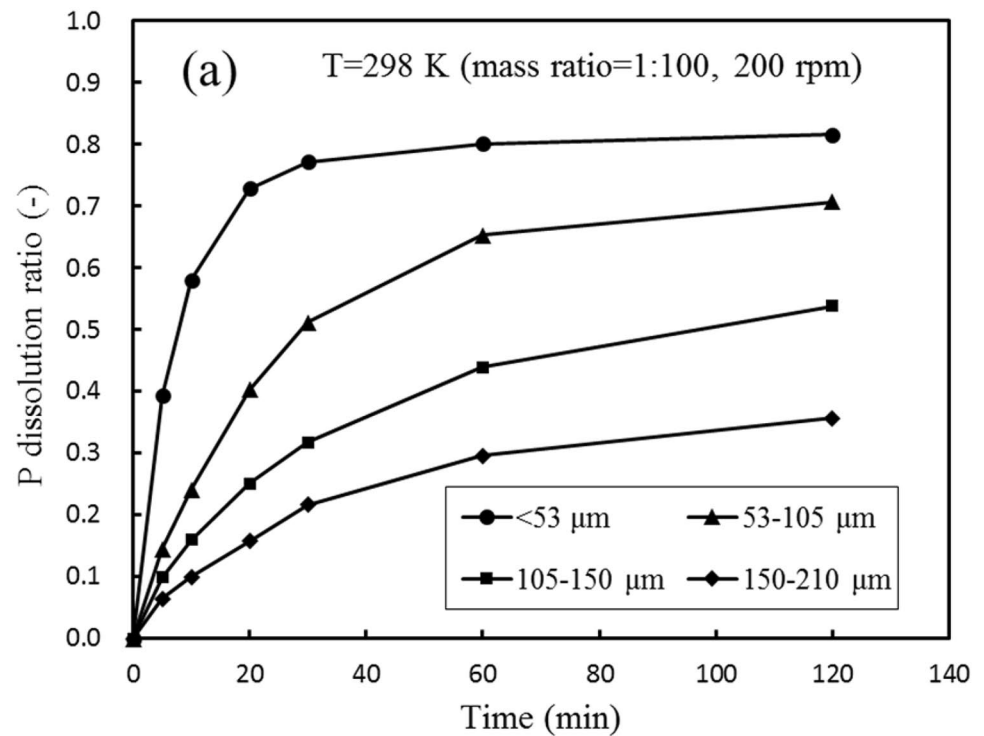
A series of leaching experiments with various parameters were conducted, and the change in the P concentration with leaching time was obtained. The dissolution ratio of each element from slag was defined as follows:

$$\eta_X = \frac{1000 \cdot C_X \cdot V \cdot M_{XO}}{w_{XO} \cdot m \cdot M_X} \quad (1)$$

where η_X is dissolution ratio of element X from slag; C_X is the X concentration in solution, mg/L; V is the final volume of leachate, L; M is the molar mass; w_{XO} is the mass percent of MO in slag; m is the mass of input slag, g.

Figure 3a presents the effect of particle size on the P dissolution ratio with a mass ratio of 1:100 and stirring speed of 200 rpm at 298 K. Dissolution reaction mainly occurred in the early stage, resulting in a rapid increase of P dissolution ratio; after 60 min, the P dissolution ratio increased slightly. Particle size had a significant effect on P dissolution. It is shown that as particle size increased, the P dissolution ratio decreased. In addition, smaller particles could reach a certain dissolution ratio in a shorter time. In the case of particle size ranging from 150 to 210 μm , the P dissolution ratio was only 35.7% after 120 min, indicating that a large amount

Fig. 3 a Effect of particle size on the change in the P dissolution ratio with leaching time; **b** dissolution ratio of each element from slag with various particle sizes after 120 min



of P-bearing solid solution hidden in slag particle did not dissolve. When particle size decreased to less than 53 μm , the P dissolution ratio increased to 81.6% after 120 min, demonstrating that most of the P-bearing solid solution was dissolved.

To fully understand slag dissolution, the dissolution ratio of each element after 120 min was calculated and is shown in Fig. 3b. In each case, the dissolution ratios of Ca, Si, and P were far higher than those of Fe, Mn, and Al. The dissolution ratio of each element increased with the decrease

in particle size; however, the Fe dissolution ratio was still low, less than 0.5%, despite of small particle size. Because Ca, Si, and P were primarily distributed in C_2S – C_3P solid solution and merwinite, it indicated that these phases were easily dissolved while the dissolution of magnesioferrite was negligible. For the slag with particle size less than 53 μm , besides P, almost all the Ca were dissolved, and the Si dissolution ratio reached 75.4%. More than 30% of Mg was also dissolved, attributing to a large dissolution of merwinite. These results show that decreasing particle size is crucial to achieve an improved selective leaching of P from slag.

Effect of temperature on the change in the P dissolution ratio from slag (< 53 μm) with a mass ratio of 1:100 and stirring speed of 200 rpm is shown in Fig. 4a. The changing trend of P dissolution ratio was similar as leaching time increased at various temperatures. The P dissolution ratio increased significantly during the first 30 min, and then increased slowly until approaching a stable value. When temperature varied from 278 to 333 K, the P dissolution ratio increased from 80.6 to 84.8% after 120 min. Although increasing temperature had a little improvement in the P dissolution ratio, it could accelerate P dissolution. Using the P concentration at 5 min, we calculated the average P dissolution rate in 5 min. It showed that the P dissolution rate was 9.8 mg/(L·min) at 278 K, while it increased approximately 1.5 time at 333 K, reaching 14.5 mg/(L·min). Although acid leaching reaction is an exothermic reaction, increasing temperature still plays a certain role in promoting P dissolution, mainly because a higher temperature facilitates mass transfer, and thus promotes the reaction between acid and C_2S – C_3P solid solution.

Figure 4b shows the dissolution ratios of major elements at various temperatures after 120 min. The Ca dissolution ratio was the highest in each case. As temperature increased, the Ca dissolution ratio increased slightly, in line with that of P. Some researches previously reported that temperature had a great influence on the iron loss of high-P iron ores and steelmaking slag during acid leaching [6, 21]. However, in this study, the Fe dissolution ratio was still very low regardless of temperature, illustrating that the Fe-bearing phase in this slag was resistant to dissolution under this condition, which was beneficial for following phosphorus recovery and residue reutilization. Si showed a totally different dissolution behavior with other elements. When temperature increased from 278 to 333 K, the Si dissolution ratio decreased from 79.1 to 56.8%. Because this leachate contained less impurities, appropriately increasing temperature facilitated P recovery from leachate in this process.

Leaching experiments whose stirring speed ranged from 20 to 300 rpm were conducted to determine the effect of agitation intensity, with mass ratio of 1:100 at 298 K. As seen in Fig. 5a, stirring speed had a significant influence on P dissolution, especially in the range of low stirring

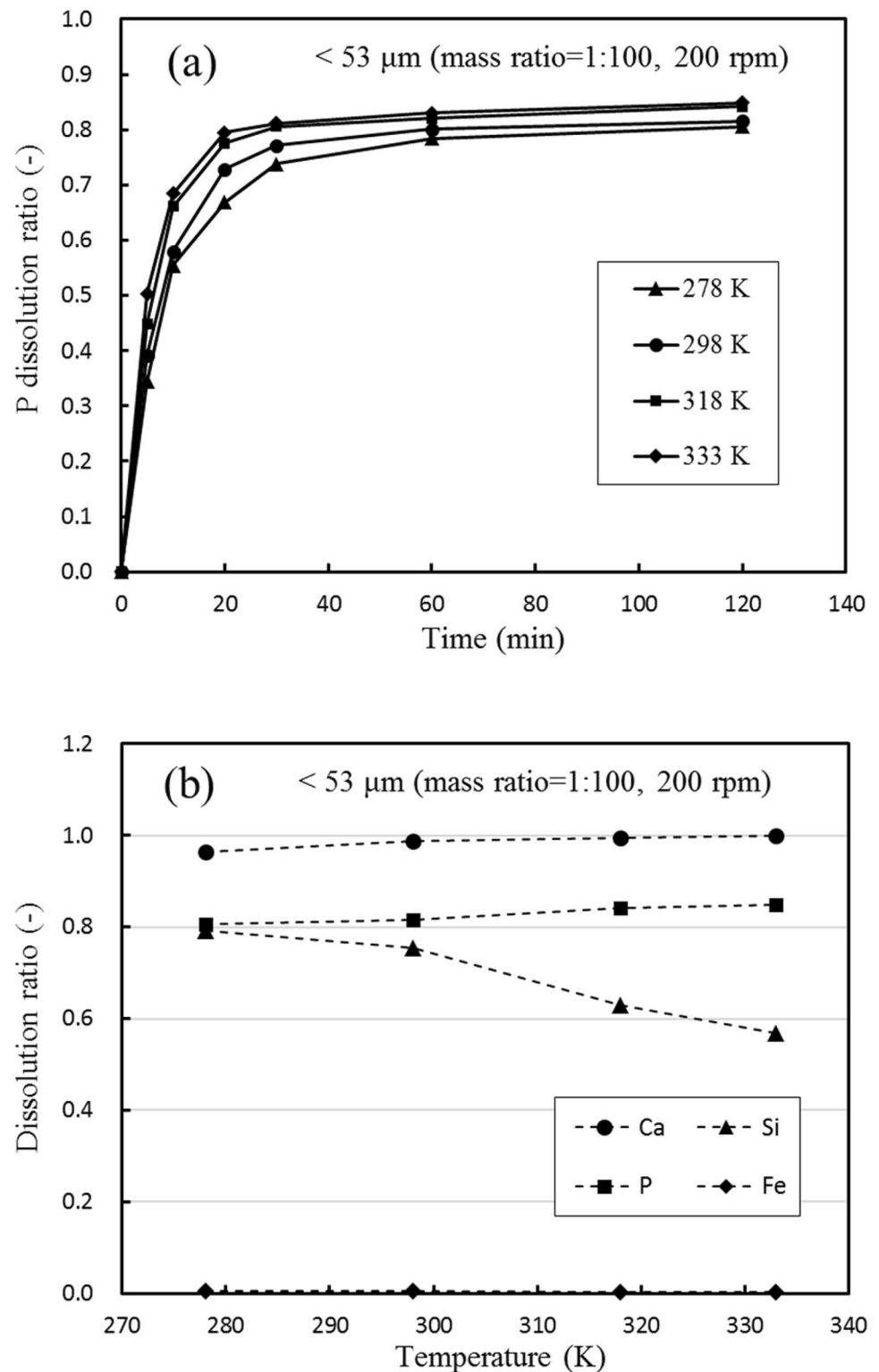
speed. When stirring speed was set as 20 rpm, most of the slag did not suspend in the solution while accumulated on the bottom of reactor, resulting in an insufficient contact between slag particles and solution. Thus, the P dissolution ratio was only 63.2% after 120 min. As stirring speed increased, P dissolution was promoted, and the P dissolution ratio could reach a high level in a shorter time. The reason was considered that improving stirring intensity accelerated mass transfer and diffusion of reactants during acid leaching. However, when stirring speed increased from 200 to 300 rpm, the P dissolution ratio increased slightly, indicating that mass transfer was not the limiting factor at 200 rpm or above. From a perspective of energy saving, stirring speed of 200 rpm was enough to ensure an efficient P dissolution.

The dissolution behavior of various elements under different stirring speeds is shown in Fig. 5b. The dissolution ratios of Ca, Si, and P increased with the stirring speed, while Fe did not dissolve. In the case of lower stirring speed (20 and 100 rpm), the slag dissolution was insufficient. To achieve a better selective leaching of P, it is necessary to choose an appropriate stirring speed to make slag particles fully contact with acid solution.

To reduce production costs and improve dissolution efficiency, we increased the mass ratio of slag to solution and investigated the P concentration in the leachate. As shown in Fig. 6a, dotted lines represent the P concentration in the solution, and solid lines describe the calculated P dissolution ratio. The P concentration in the leachate increased with the mass ratio of slag to solution. When the mass ratio varied from 1:100 to 1:10, the P concentration increased from 116.1 to 926.8 mg/L after 120 min. The P dissolution ratio showed similar variation trend under various mass ratios. However, as the mass ratio increased, the P dissolution ratio decreased slightly. In the case of mass ratio of 1:10, only 74.7% of P was dissolved from slag. In addition, the P dissolution ratio was extremely low in the beginning. This was because a large amount of Ca was dissolved from slag, and the pH control system was not incapable of supplying enough acid solution to rapidly decrease solution pH to the target value. Although increasing the mass ratio had a negative effect on P dissolution, a large amount of P in slag was virtually dissolved even at a mass ratio of 1:10.

Figure 6b shows the dissolution ratios of major elements with various mass ratios. As mass ratio increased, the dissolution ratios of Ca and P decreased slightly, and Fe dissolution did not change, while Si dissolution was suppressed significantly. When mass ratio increased to 1:10, the Si dissolution ratio decreased approximately two times, only 42.3%. Overall, increasing mass ratio of slag to liquid was beneficial for improving productivity and following phosphorus recovery, but inevitably sacrificed a portion of P dissolution.

Fig. 4 a Effect of temperature on the change in the P dissolution ratio with leaching time; **b** dissolution ratios of elements from slag at different temperatures after 120 min

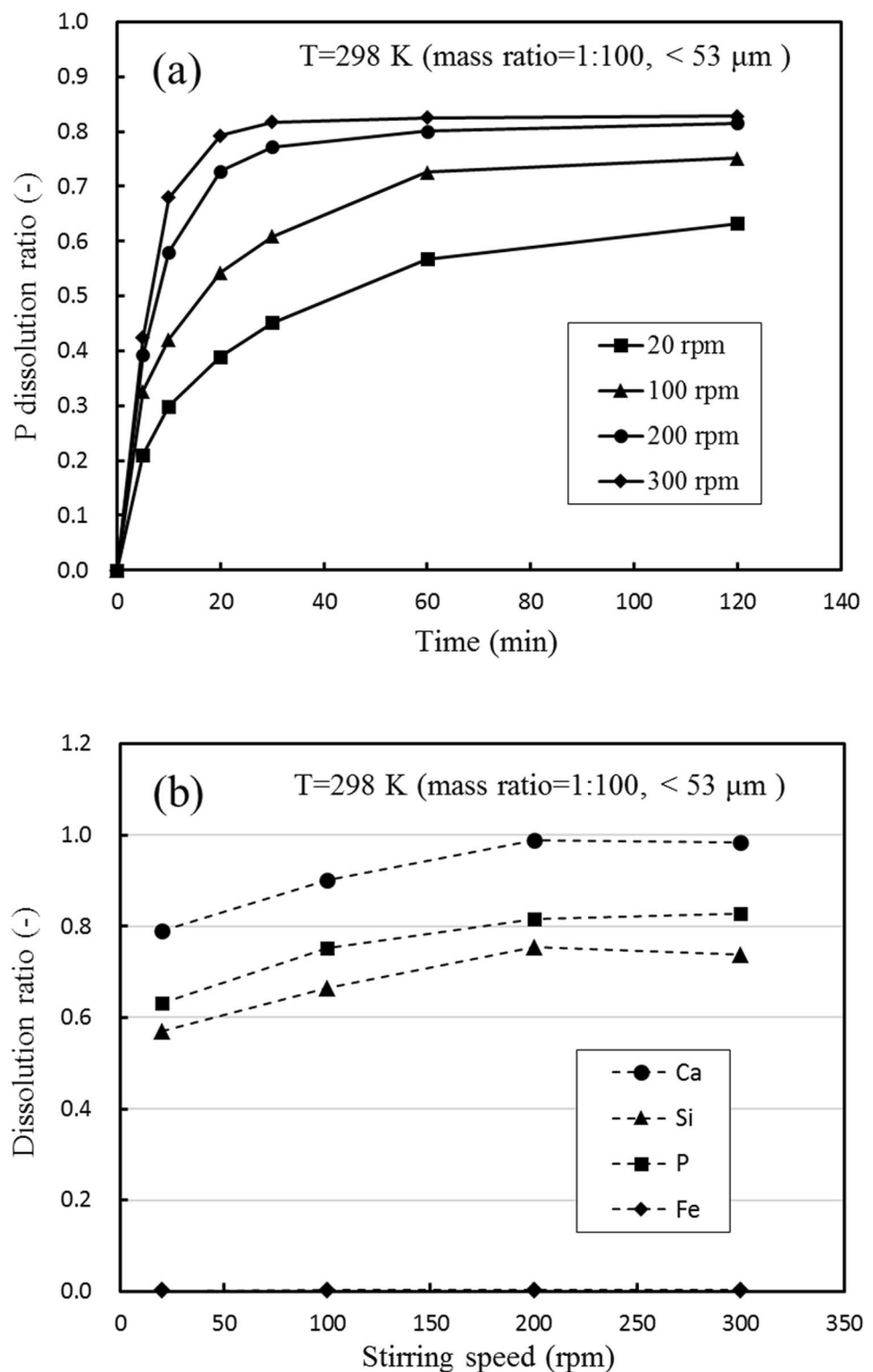


Characterization of Residue After Leaching

The morphology of residues under different leaching conditions is present in Fig. 7, and Table 3 lists the composition of typical mineral phases on the residue surface.

Residue A consisted of some fine particles with holes and bigger particles with single phase; the major phase on their surface principally containing Fe, Mg, and Mn was magnesioferrite; it was difficult to detect the P-bearing solid solution and merwinite. In the case of large particle size,

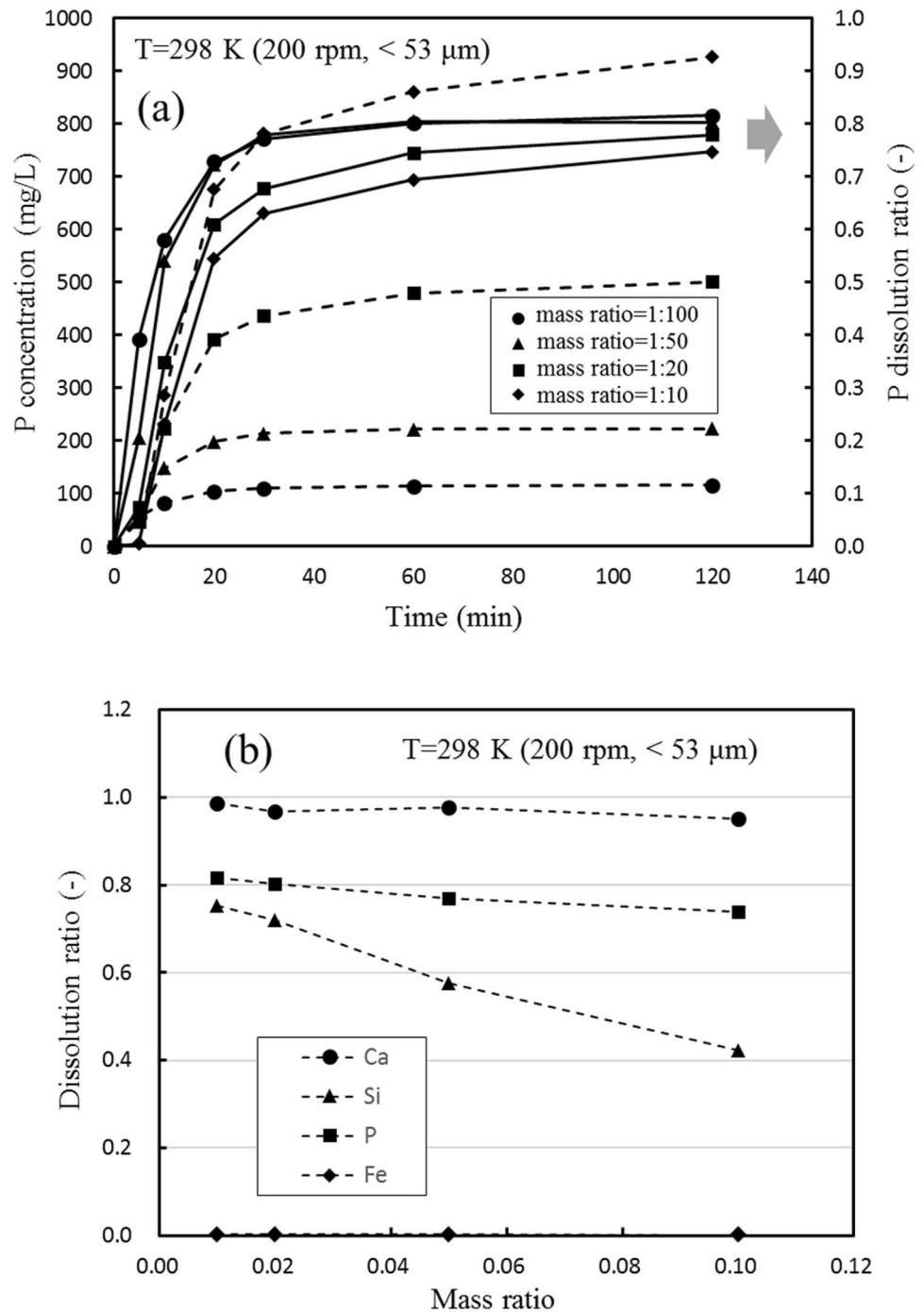
Fig. 5 a Effect of stirring speed on the change in the P dissolution ratio with leaching time; **b** dissolution ratios of elements from slag at various stirring speeds after 120 min



residue B presented a rough and porous surface; the white phase was magnesioferrite; the major elements detected in these holes were Si and Fe. When mass ratio was high, there were two mineral phases found on the surface of residue C, including magnesioferrite; the gray phase with high

Si content seemed to wrap around residue particles. These results demonstrated that C_2S-C_3P solid solution and merwinite was readily dissolved compared to the magnesioferrite. Most of the P in slag could be effectively separated.

Fig. 6 a Effect of mass ratio on the change in the P concentration and P dissolution ratio with leaching time; **b** dissolution ratios of elements from slag under different mass ratios after 120 min



As shown in Fig. 8, XRD results revealed that the original slag mainly consisted of magnesioferrite, solid solution, and merwinite. Because calcium silicate ($\text{C}_2\text{S}-\text{C}_3\text{P}$) and merwinite (C_3MS_2) had similar structures, their peaks were almost identical. After leaching, the peaks associated with calcium silicate and merwinite weakened significantly, whereas those of magnesioferrite intensified, demonstrating that solid solution and merwinite was largely dissolved and magnesioferrite remained in the residue, in line with above analysis.

Compared with residues B and C, the peaks associated with calcium silicate and merwinite in the residue A were the lowest, indicating that more solid solution was separated. Due to removal of the P-bearing phase, the residue primarily consisting of magnesioferrite had the potential to serve as a flux in steelmaking process, which represented a major step forward in utilization of steelmaking slag.

Table 4 lists the average composition of residues under different leaching conditions. Compared with the composition of

Fig. 7 EPMA images of residues under different leaching conditions

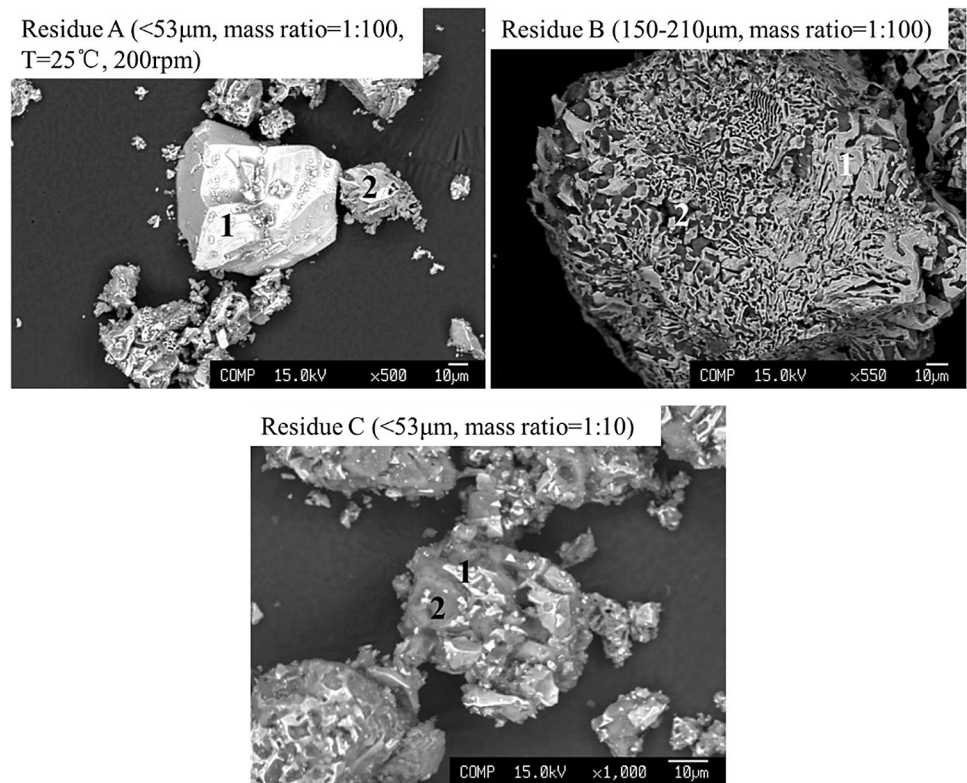


Table 3 Average composition of major phase on the residue surface (mass%)

| | | Ca | Si | Fe | P | Mn | Mg |
|-----------|---|-----|------|------|-----|-----|------|
| Residue A | 1 | 0.9 | 0.0 | 48.4 | 0.0 | 9.1 | 8.9 |
| | 2 | 0.5 | 0.3 | 43.2 | 0.0 | 7.4 | 11.5 |
| Residue B | 1 | 0.5 | 0.3 | 44.3 | 0.0 | 7.3 | 10.8 |
| | 2 | 2.2 | 32.8 | 5.2 | 0.6 | 0.8 | 0.6 |
| Residue C | 1 | 0.8 | 1.5 | 42.4 | 0.2 | 6.6 | 9.7 |
| | 2 | 3.2 | 28.8 | 6.5 | 0.8 | 0.9 | 1.1 |

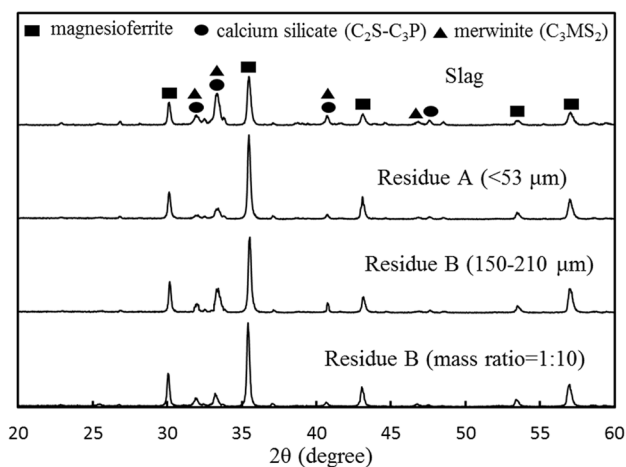
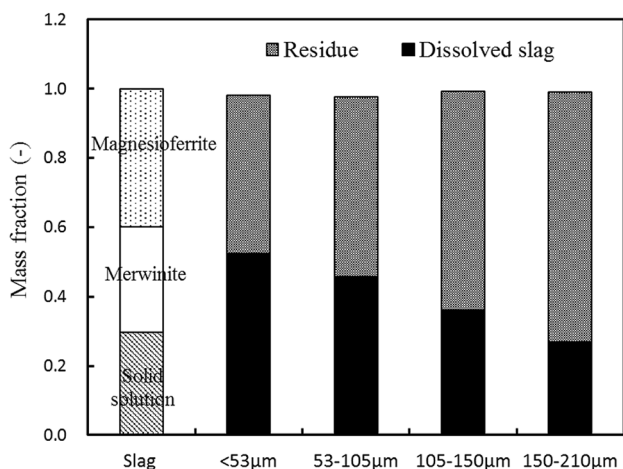


Fig. 8 XRD patterns of original slag and its residues

original slag, the CaO and P₂O₅ contents decreased while the Fe₂O₃ content increased correspondingly. In the case of large particles, the P₂O₅ content in the residue was still high due to an insufficient dissolution of solid solution. The SiO₂ content in the residue C was relatively high, resulting from a lower Si dissolution ratio, and the P₂O₅ content was 1.61%. Because a better selective leaching was achieved, residue A containing 0.84% P₂O₅ and 61.73% Fe₂O₃ could be used in steel plant. Therefore, decreasing the mass ratio of slag to solution was beneficial for residue reutilization.

Table 4 Average composition of residues under different leaching conditions (mass%)

| | CaO | SiO ₂ | Fe ₂ O ₃ | P ₂ O ₅ | MgO | MnO | Al ₂ O ₃ |
|---|-------|------------------|--------------------------------|-------------------------------|-------|------|--------------------------------|
| Residue A (< 53 μm, mass ratio = 1:100) | 1.04 | 6.33 | 61.73 | 0.84 | 14.45 | 9.27 | 6.34 |
| Residue B (150–210 μm, mass ratio = 1:100) | 23.31 | 15.82 | 38.29 | 2.92 | 9.59 | 5.90 | 4.17 |
| Residue C (< 53 μm, mass ratio = 1:10) | 5.30 | 22.76 | 47.97 | 1.61 | 10.01 | 7.17 | 5.18 |

**Fig. 9** Mass fraction of each phase in slag in comparison to those of the dissolved slag and residue

Discussion

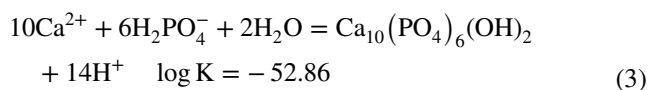
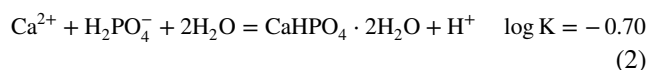
Dissolution Behavior of Mineral Phases

To gain insight into selective leaching of P, we calculated the mass fraction of each phase in slag by using the same method described in previous paper [20] and compared these results with the mass fractions of residue and dissolved slag. As shown in Fig. 9, slag was comprised of approximately 30% of solid solution, 30% of merwinite, and 40% of magnesioferrite. The results in Fig. 3b showed that solid solution had a higher solubility in acid solution and the solubility of magnesioferrite was extremely low. Because of a higher Mg dissolution ratio, it was concluded that merwinite was easily dissolved, similar with dicalcium silicate, which was also confirmed by Zhu et al. [22]. In the case of particle size between 150 and 210 μm, only 26.8% of slag was dissolved, far lower than the sum of mass fractions of solid solution and merwinite, indicating that these phases did not dissolve well. This was because a part of solid solution and merwinite was wrapped in the particle and could not contact with acid solution. As particle size decreased, the mass fraction of dissolved slag increased significantly. When particle size was less than

53 μm, more than half of slag was dissolved, and this value approached the sum of mass fractions of solid solution and merwinite, illustrating that most of these phases was dissolved, and the residue principally consisted of magnesioferrite. Therefore, to achieve a better selective leaching, slag should be ground to smaller particles and make each phase fully contact with acid solution.

Dissolution Behavior of P and Si

When we investigate the effect of mass ratio of slag to liquid, it is necessary to estimate the saturated P concentration in leachate and the possibility of phosphate precipitation. Because of a high Ca concentration, the reactions between Ca²⁺ and phosphate ions in leachate were considered. CaHPO₄·2H₂O and Ca₁₀(PO₄)₆(OH)₂ were the common precipitates present in this system, and their reactions were expressed in Eqs. (2) and (3) [17, 20]. In this acidic solution, phosphate ions primarily existed in the form of H₂PO₄⁻ [23]. We assumed activity coefficients of ions as 1, and then calculated solubility lines of these two kinds of precipitates at pH 3. In Fig. 10, CaHPO₄·2H₂O had priority to precipitate, and the saturated P concentration decreased with the increase in Ca concentration. Leaching results with different mass ratios were also plotted in this figure. In the case of mass ratio of 1:10, the Ca and P concentrations in leachate were the highest, reaching 18,306.4 mg/L and 926.8 mg/L, respectively. The result for this leachate located below the solubility line of CaHPO₄·2H₂O, indicating that phosphate precipitation hardly occurred, and phosphate ions could stably exist in this leachate. Therefore, selective leaching of P could be achieved in a broad range of concentration.



During leaching at a high mass ratio or temperature, the dissolution behavior of Si showed an interesting phenomenon. Because almost all the Ca was dissolved, it demonstrated that most of the solid solution and merwinite was

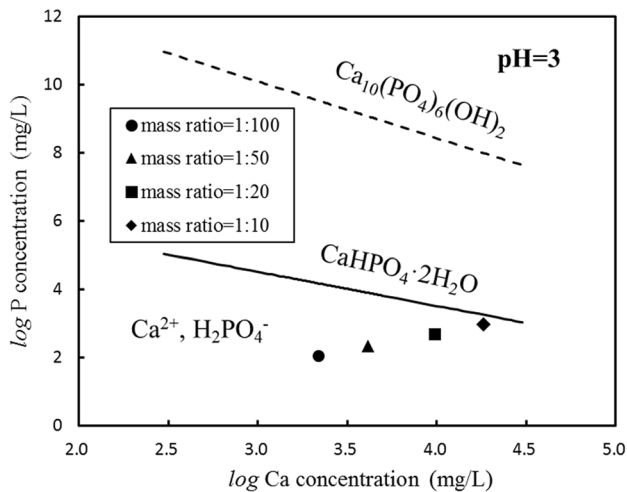


Fig. 10 Solubility lines of calcium phosphates at pH 3 and leaching results

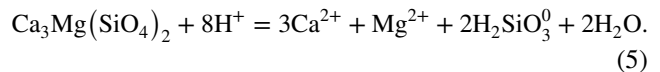
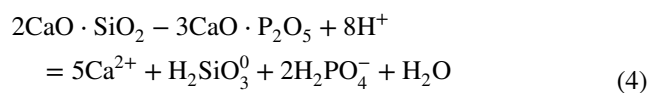
dissolved, while the Si dissolution ratio was far lower than that of Ca. The dissolved Si existed in the form of H_2SiO_3^0 in the solution and monosilicic acid could polymerize to form discrete particles [23, 24]. Colloidal silica is a stable aqueous dispersion or sol of discrete amorphous silica particles having diameters of 1–100 nm. They may remain for long time without significant settling or loss of stability. Silica sols can be destabilized by aggregation, gelation, crystallization, or particle growth plus settling. Aggregation occurs by coagulation in which colloidal silica particles collide or by flocculation in which particles become linked by bridges of flocculating agent [24]. In this study, when mass ratio was high, the Si concentration was high, resulting in the formation of large amounts of colloidal silica particles. They were easier to collide and aggregate than that in the dilute solution. The Si-rich phase detected on the surface of residue C could confirm this. In addition, it was reported that aggregation and precipitation of colloidal silica particles was favored by high temperature [25]. Therefore, in these conditions, the aggregated colloidal silica particles could form silica gel, and then precipitated, resulting in a lower Si dissolution ratio. The removal of Si by forming silica gel was beneficial for the following P recovery from leachate.

Kinetics Analysis

For a reaction between solid and liquid, its rate is generally controlled by diffusion through the product layer, the chemical reaction on particle surface or a mixed of diffusion and chemical reactions. The overall reactions for slag dissolution can be expressed as follows:

Table 5 Regression coefficients for kinetics models

| Parameters | $1 - (1 - x)^{1/3}$ | $1 - \frac{3(1 - x)^{2/3} + 2(1 - x)}{3}$ |
|-----------------------|---------------------|---|
| < 53 μm | 0.8734 | 0.9611 |
| 53–105 μm | 0.9361 | 0.9912 |
| 105–150 μm | 0.9444 | 0.9969 |
| 150–210 μm | 0.9435 | 0.9928 |
| 278 K | 0.8816 | 0.9717 |
| 298 K | 0.8734 | 0.9611 |
| 318 K | 0.8953 | 0.9736 |
| 333 K | 0.8735 | 0.9706 |



Considering that slag can be viewed as spherical particles and slag particle gradually shrunk, shrinking core model is selected in this study. The unreacted residue around the core is considered as the solid diffusion layer. When the diffusion of reagent through the residue layer is the rate-controlling step, Eq. (6) of the shrinking core model is achieved to describe the dissolution kinetics. If the leaching process is controlled by the surface chemical reaction, the rate of reaction of shrinking core model can be expressed as Eq. (7) [26–28].

$$1 - 3(1 - x)^{2/3} + 2(1 - x) = \frac{6bDC_P}{\rho_B r_0^2} t = k_d t \quad (6)$$

$$1 - (1 - x)^{1/3} = \frac{bk_c C_P}{\rho_B r_0} t = k_r t, \quad (7)$$

where x is the P dissolution ratio, C_P is the P concentration in leachate (g/cm^3), D is the diffusion coefficient in the residue layer (cm^2/s), b is the stoichiometric coefficient, r_0 is the initial radius of slag particle (cm), t is the leaching time (s), ρ_B is the solid density (g/cm^3), k_c is the chemical rate constant (cm/s), k_d and k_r are the apparent rate constants (1/s) which are calculated from Eqs. (6) and (7), respectively.

To determine the kinetic parameters and rate-controlling step of selective leaching of P from dephosphorization slag, the P dissolution ratio with various particle sizes and at different temperatures was analyzed based on shrinking core model, respectively. Because slag dissolution primarily occurred in the beginning, we selected the leaching

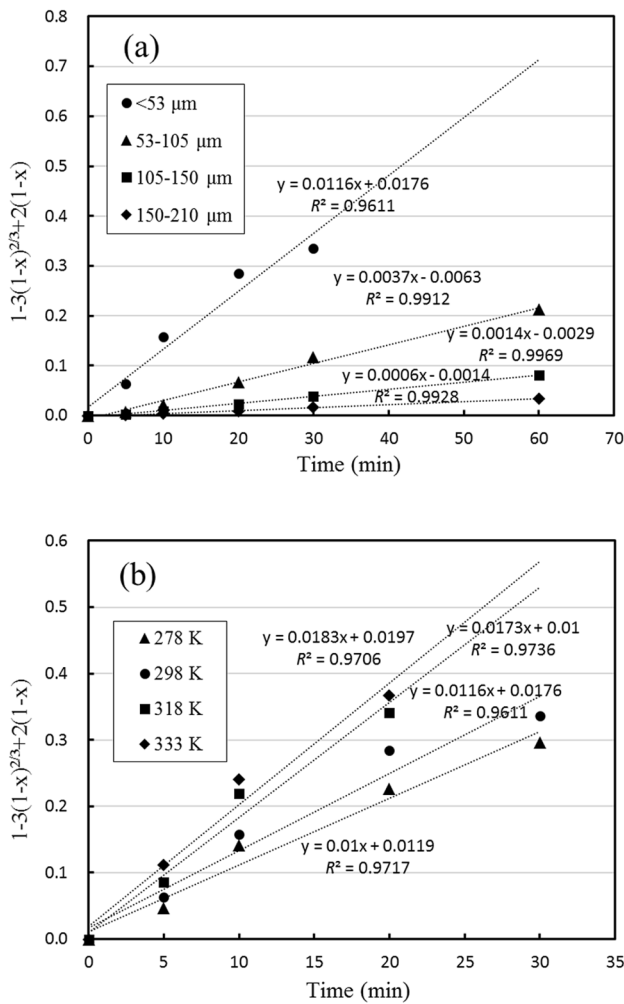


Fig. 11 The variation in $1-3(1-x)^{2/3}+2(1-x)$ with leaching time **a** with different particle sizes; **b** at different temperatures

results in 30 min. Leaching results were fitted with Eqs. (6) and (7). The calculated correlation coefficients (R^2) are listed in Table 5. The highest regression coefficient was obtained for the type of diffusion control. There was a good correlation between the P dissolution ratio and Eq. (6), and nearly zero point intercepts were obtained, as shown in Fig. 11. These results illustrated that the dissolution rate of P from slag was controlled by diffusion in the residue layer. The apparent rate constants (k_d) were calculated as slopes of the straight lines. With the increase in particle size, the diffusion rate decreased significantly. A higher temperature resulted in a higher diffusion rate.

Equation (6) reveals that in the case of diffusion control, apparent rate constants are directly proportional to $1/d^2$. Figure 12 plots the apparent rate constant obtained in Fig. 11a as a function of $1/d^2$, where d is the diameter of initial slag particle. It showed a linear relationship between k_d versus

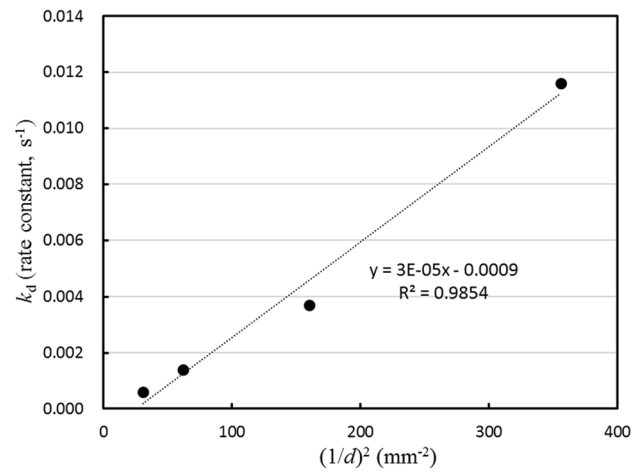


Fig. 12 Plot of k_d as a function of $(1/d)^2$

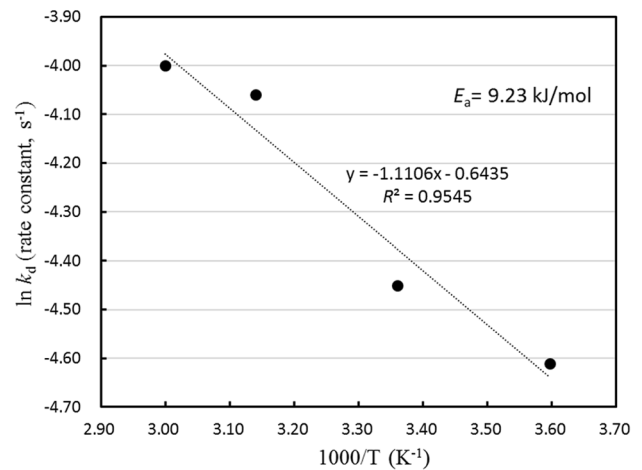


Fig. 13 Arrhenius plot of $\ln k_d$ against $1/T$

$1/d^2$, confirming that the diffusion in the residue layer was the rate-controlling step.

Using the apparent rate constants k_d obtained by application of Eq. (6), the Arrhenius plot was obtained. As shown in Fig. 13, the Arrhenius plot was a straight line constructed with the $\ln k_d$ against $1/T$, and its slope was $(-E_a/R)$. The activation energy calculated in this study was 9.23 kJ/mol. In some leaching studies [27–29], high value of activation energy generally indicates that the chemical reaction would be the rate-controlling step and low activation energy indicates that the diffusion in the product layer could be rate-controlling step. The activation energy of a diffusion-controlled process was characterized as being 4.18 to 12.56 kJ/mol, while the activation energy for a chemically controlled process was usually greater than 41.86 kJ/mol [30]. As the activation energy was 9.23 kJ/mol, this result proved that the P dissolution from slag was controlled by diffusion in the

residue layer. In this case, two diffusion processes competed in determining the reaction rate: (1) diffusion of H^+ from HCl; (2) diffusion of $H_2PO_4^-$ produced by the surface chemical reaction. The diffusion rate of H^+ was presumed to be fast due to its relatively small size compared to $H_2PO_4^-$ [29]. Accordingly, the diffusion of $H_2PO_4^-$ was considered as the rate-controlling step of dissolution reaction.

Conclusion

To efficiently recover P and reuse P-removal residue, we adopted selective leaching of P from dephosphorization slag. In the present study, the effects of leaching parameters on the dissolution behavior of slag in the HCl solution were investigated. It was determined that with the decrease in particle size and increase in stirring speed, the P dissolution ratio increased significantly, and a higher dissolution rate was obtained. When particle size was less than 53 μm and stirring speed exceeded 200 rpm, most of the P-bearing C_2S – C_3P solid solution was dissolved, achieving an improved selective leaching of P.

Increasing temperature and decreasing the mass ratio of slag to liquid had a slight influence on promoting P dissolution, while the Si dissolution was significantly suppressed in the case of high temperature and mass ratio due to the formation of silica gel. The P dissolution ratio could reach 84.9%, and the Fe dissolution was negligible. Because C_2S – C_3P solid solution and merwinite was dissolved sufficiently, the residue primarily containing magnesioferrite could be used as a flux in steel plant.

A shrinking core model with diffusion in the product layer as the rate-controlling step was successfully used to describe the dissolution kinetics of P. As temperature increased, apparent rate constant increased slightly. The calculated activation energy was 9.23 kJ/mol, demonstrating that the P dissolution from slag was controlled by diffusion in the residue layer.

Acknowledgement This work was supported by JST-Mirai Program Grant Number JPMJMI17C2, Japan.

Compliance with Ethical Standards

Conflict of interest On behalf of all authors, the corresponding author states that there is no conflict of interest.

References

1. Tonini D, Saveyn H, Huygens D (2019) Environmental and health co-benefits for advanced phosphorus recovery. *Nat Sustain* 2:1051–1061
2. Roy ED (2017) Phosphorus recovery and recycling with ecological engineering: a review. *Ecol Eng* 98:213–227
3. Zou H, Wang Y (2016) Phosphorus removal and recovery from domestic wastewater in a novel process of enhanced biological phosphorus removal coupled with crystallization. *Bioresour Technol* 211:87–92
4. Blocher C, Niewersch C, Melin T (2012) Phosphorus recovery from sewage sludge with a hybrid process of low pressure wet oxidation and nanofiltration. *Water Res* 46:2009–2019
5. Matsubae K, Yamasue E, Inazumi T, Webeck E, Miki T, Nagasaka T (2016) Innovations in steelmaking technology and hidden phosphorus flows. *Sci Total Environ* 542:1162–1168
6. Wang H, Li G, Zhao D, Ma J, Yang J (2017) Dephosphorization of high phosphorus oolitic hematite by acid leaching and the leaching kinetics. *Hydrometallurgy* 171:61–68
7. Kitamura S, Miyamoto K, Shibata H, Maruoka N, Matsuo M (2009) Analysis of dephosphorization reaction using a simulation model of hot metal dephosphorization by multiphase slag. *ISIJ Int* 49:1333–1339
8. Matsui A, Nakase K, Kikuchi N, Kishimoto Y, Takahashi K, Ishida K (2011) Phosphorus separation from steelmaking slag by high temperature reduction with mechanical stirring. *Tetsu-to-Hagané* 97:416–422
9. Zhang X, Chen J, Jiang J, Li J, Tyagi RD, Surampalli RY (2020) The potential utilization of slag generated from iron and steelmaking industries: a review. *Environ Geochem Health* 42:1321–1334
10. Matsubae-Yokoyama K, Kubo H, Nakajima K, Nagasaka T (2009) A material flow analysis of phosphorus in Japan. *J Ind Ecol* 13:687–705
11. Pahlevani F, Kitamura S, Shibata H, Maruoka N (2010) Distribution of P_2O_5 between solid solution of $2CaO-SiO_2-3CaO-P_2O_5$ and liquid phase. *ISIJ Int* 50:822–829
12. Kubo H, Matsubae-yokoyama K, Nagasaka T (2010) Magnetic separation of phosphorus enriched phase from multiphase dephosphorization slag. *ISIJ Int* 50:59–64
13. Li C, Gao J, Guo Z (2016) Isothermal enrichment of P-concentrating phase from $CaO-SiO_2-FeO-MgO-P_2O_5$ melt with super gravity. *ISIJ Int* 56:759–764
14. Koizumi S, Miki T, Nagasaka T (2016) Enrichment of phosphorus oxide in steelmaking slag by utilizing capillary action. *J Sustain Metall* 2:38–43
15. Teratoko T, Maruoka N, Shibata H, Kitamura S (2012) Dissolution behavior of dicalcium silicate and tricalcium phosphate solid solution and other phases of steelmaking slag in an aqueous solution. *High Temp Mater Proc* 31:329–338
16. Numata M, Maruoka N, Kim SJ, Kitamura S (2014) Fundamental experiment to extract phosphorus selectively from steelmaking slag by leaching. *ISIJ Int* 54:1983–1990
17. Du C, Gao X, Ueda S, Kitamura S (2017) Effect of Na_2O addition on phosphorus dissolution from steelmaking slag with high P_2O_5 content. *J Sustain Metall* 3:671–682
18. Du C, Gao X, Ueda S, Kitamura S (2018a) Effect of $Fe^{2+}/T.Fe$ ratio on the dissolution behavior of P from steelmaking slag with high P_2O_5 content. *J Sustain Metall* 4:443–454
19. Du C, Gao X, Ueda S, Kitamura S (2018b) Recovery of phosphorus from modified steelmaking slag with high P_2O_5 content via leaching and precipitation. *ISIJ Int* 58:833–841
20. Du C, Gao X, Ueda S, Kitamura S (2019) Separation and recovery of phosphorus from steelmaking slag via a selective leaching–chemical precipitation process. *Hydrometallurgy* 189:105109
21. Qiao Y, Diao J, Liu D, Yang J, Guo D, Gong S, Xie B (2018) Dephosphorisation of steel slags by leaching with sulphuric acid. *Miner Process Extr Metall* 127:250–254

22. Zhu Z, Gao X, Ueda S, Kitamura S (2019) Contribution of mineralogical phases on alkaline dissolution behavior of steelmaking slag. *ISIJ Int* 59:1908–1916
23. Futatsuka T, Shitogiden K, Miki T, Nagasaka T, Hino M (2004) Dissolution behavior of nutrition elements from steelmaking slag into seawater. *ISIJ Int* 44:753–761
24. Bergna HE (1994) The colloid chemistry of silica, chapter 1. American Chemical Society, Washington, DC
25. White DE, Brannock WW, Murata KJ (1956) Silica in hot-spring waters. *Geochim Cosmochim Acta* 10:27–59
26. Abdel-Aal EA, Rashad MM (2004) Kinetic study on the leaching of spent nickel oxide catalyst with sulfuric acid. *Hydrometallurgy* 74:189–194
27. Aydogan S, Ucar G, Canbazoglu M (2006) Dissolution kinetics of chalcopyrite in acidic potassium dichromate solution. *Hydrometallurgy* 81:45–51
28. Gharabaghia M, Irannajadb M, Azadmehrb AR (2013) Leaching kinetics of nickel extraction from hazardous waste by sulphuric acid and optimization dissolution conditions. *Chem Eng Res Des* 91:325–331
29. Olanipekun E (1999) A kinetic study of the leaching of a Nigerian ilmenite ore by hydrochloric acid. *Hydrometallurgy* 53:1–10
30. Habashi F (1969) Principles of extractive metallurgy, vol 1. Gordon and Breach, New York

Publisher's Note Springer Nature remains neutral with regard to jurisdictional claims in published maps and institutional affiliations.